

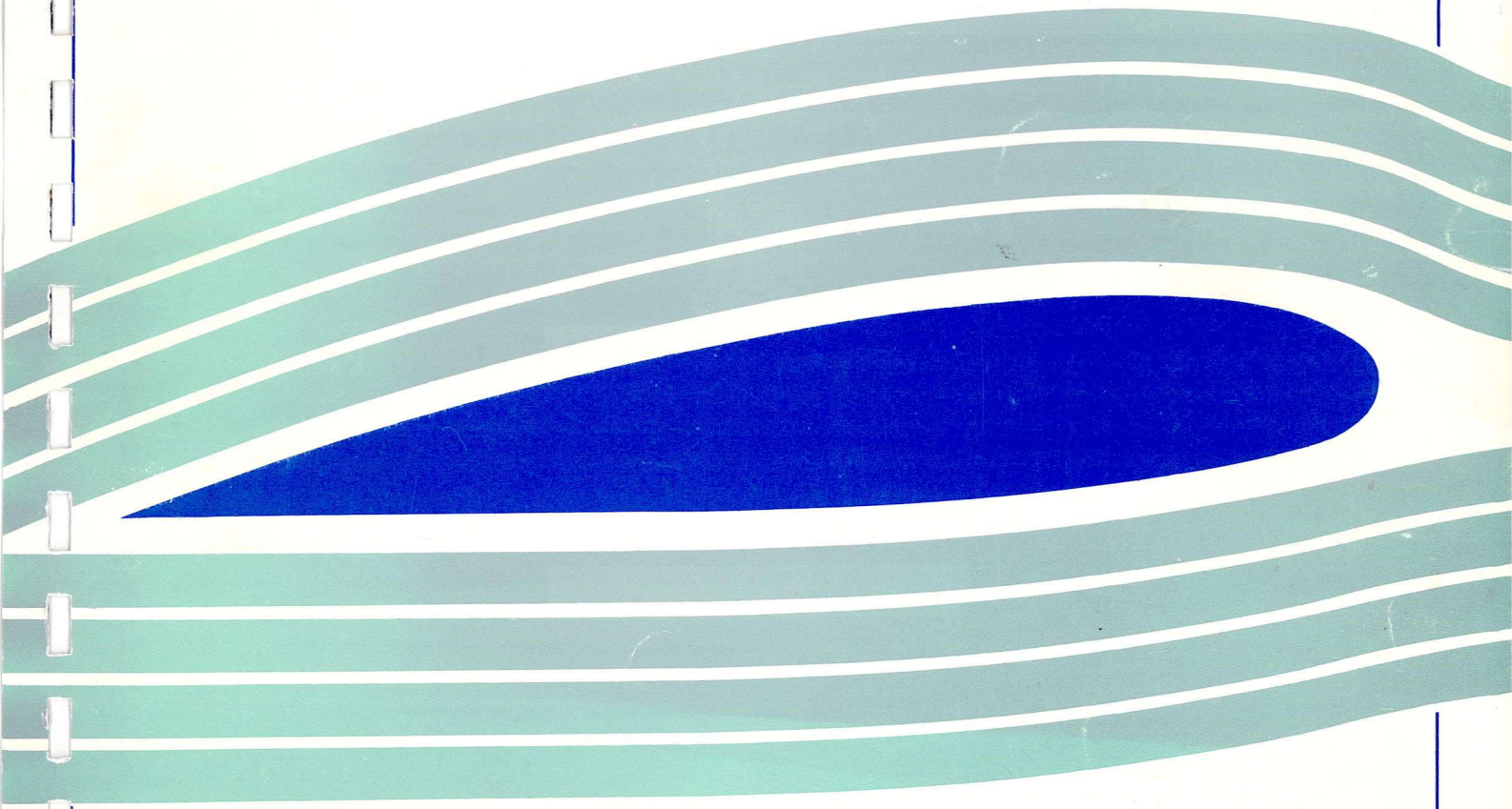


University of Glasgow
DEPARTMENT OF
**AEROSPACE
ENGINEERING**

**Summary of Beddoes/WHL
Aerodynamic Model**

Aerospace Engineering Report 0207

Jeremy Beedy



Summary of Beddoes/WHL
Aerodynamic Model

Aerospace Engineering Report 0207

Jeremy Beedy

Department of Aerospace Engineering
University of Glasgow
Glasgow G12 8QQ
United Kingdom

July 2002

Contents

1	Introduction	1
2	Derivation of Indicial Lift Function	2
3	Attached Flow Model	3
3.1	Numerical Methods	3
4	Dynamic Stall Model	7
4.1	Application of dynamic Stall Model	8
5	Region Between Attached and Dynamic Stall Models	10
5.1	Mechanisms of Separation leading to Dynamic Stall	10
5.2	Trailing Edge Separation	11
5.3	Critical Pressure Rise	14
5.4	Application of the Critical Pressure Rise	16
5.5	Deep Stall and Vortex Shedding	17
5.6	Sweep Effects and Separation Points	18
5.7	Application to Arbitrary Planform Rotor Sections	20
6	Conclusion	21

Nomenclature

Symbols	Definition	Units
A_1, A_2	Coefficients given by Jones [6]	-
AR	Aspect ratio $AR = \frac{b^2}{S}$	-
b_1, b_2	Coefficients given by Jones [6]	-
b	Semi-chord length $b = \frac{c}{2}$	m
C_L	Coefficient of Lift	-
$C_{L_\alpha}(M)$	Lift curve slope for particular Mach number	-
CP	Non-dimensional centre of pressure	-
c	Chord length	m
d_f	Function of M (For $0.3 \leq M \leq 0.8$, $4.0 \geq d_f \geq 0.5$)	-
E	Vortex dissipation	s
f	Separation point $f = \frac{x_{sp}}{c}$	-
k_0	$-0.16 \leq k_0 \leq -0.10$	-
k_1	$-0.10 \leq k_1 \leq 0.28$	-
k_2	$-0.115 \leq k_2 \leq 0.04$	-
K_D	Given by $K_D = 2.7 \exp -d_f f$	-
K_N	Kirchoff approximation	-
M	Mach number	-
P	Pressure	Nm^{-2}
\bar{q}	Non-dimensional pitch rate $q = \frac{\dot{\theta}c}{U}$	-
S	Rotor planform area	m^2
s	Non-dimensional time	-
t	Dimensional time	s
T_l	Time constant (Impulsive loading)	s
T_p	Time constant $T_p \propto M$	s
T_q	Time constant (Impulsive loading due to pitch rate)	s
U	Freestream velocity	ms^{-1}

x	Chordwise axis	m
x_{ac}	Aerodynamic centre	m
y	Spanwise axis	m

Greek Symbols	Definition	Units
α	Angle of incidence	rad
$\bar{\alpha}$	Step change in angle of incidence	rad
δ	Shock deflection angle	deg
Δ	Infinitesimal increment	-
η	Function of sweep back angle	-
Λ	Sweep back angle	deg
$\phi_c(s)$	Circulatory indicial lift function	-
$\phi_i(s)$	Impulsive indicial lift function	-
$\phi_p(s)$	Impulsive indicial lift function due to pitch rate	-
$\dot{\theta}$	Pitch rate about $\frac{3}{4}$ chord position	$rad\,s^{-1}$
ρ	Density	$kg\,m^{-3}$
θ	Shock angle	deg
τ	Vortex time $0 \leq \tau \leq T_{v_1}$	s

Subscripts	Definition
1	Upstream values (shock)
2	Downstream values (shock)
∞	Freestream values
<i>ac</i>	Aerodynamic centre
<i>AM</i>	Apparent mass terms
<i>DD</i>	Divergence angle For $0.3 \leq M \leq 0.8$, $10.3 \geq \alpha_{DD} \geq 0$
<i>MV</i>	Moment due to vortex
<i>NV</i>	Normal force due to vortex
<i>n</i>	Sampling steps
<i>sp</i>	Separation point
<i>v</i>	Vortex terms
Superscripts	Definition
'	Compressibility effects included

1 Introduction

The aerodynamic model developed by Tom Beddoes [1], in conjunction with WHL, was aimed at calculating the unsteady aerodynamic forces encountered in helicopter rotor operating environments. The method was developed based on several criteria including simplicity to allow for quick computational times, incorporation of both attached flow conditions and separated flow conditions and the ability to include arbitrary forcing functions. The need to include arbitrary forcing terms originates from the phenomenon of blade vortex interaction which occurs mainly in forward and manoeuvring flight. In these operating environments, the aerodynamic forcing on the blades is often out of phase with the blade response, and this can result in resonance and flutter. Also the encountering of wake vortices can excite higher natural frequencies, and have the same undesired effect. The interaction between blades and vortices can also result in large changes in incidence due to the induced velocity, which can in turn cause a large increase in the lift and pitching moment, or cause the blade to stall locally.

Based on these criteria, the model assumed the form of an indicial response function for the attached flow regions. For the separated flow regions, another approach is taken. This part of the model is based purely on empirical observations of dynamic stall on aerofoil sections. These two approaches allow for the calculation of the lift and pitching moments due to variations in the incidence of aerofoil sections and the Mach number of the flow as a function of both time and azimuth angle. The effects of supercritical flow for both transonic and high incidence aerofoil conditions are included in this model [2]. Also the effects of leading edge and trailing edge separation and the effects of these phenomena on the pressure distributions are accounted for. The effects of stall vortex shedding on the lift and pitching moment are modeled using a critical pressure rise criterion. Further developments include

the ability to handle arbitrary planforms and 3-dimensional effects including spanwise separation points based on a method developed by Küchemann. These inclusions extend the viable range of rotor conditions that can be handled by the method. While this method for rotor load calculations is quick, there are a number of issues that are not addressed. These include the incorporation of the 3-Dimensional viscous effects in the tip region, and the effects of span-wise flows along the blades during flight operations.

2 Derivation of Indicial Lift Function

The Indicial Lift Functions which form the basis of this numerical model are constructed from exponential functions in time [3]. This approach allows for a simple derivation of the response using Laplacian transformations to give the lift transfer functions. Also this approach allows for the calculation of arbitrary forcing of the blades using a superposition procedure. The non-dimensional time is given by:

$$s = \frac{2tU}{c} \quad (1)$$

Where $\frac{2U}{c}$ is the time required for the airfoil to travel a distance of one semi-chordlength. The equation (1) is further modified to account for Mach number effects using the Prandtl-Glauert transformation [8]:

$$s' = s(1 - M^2) \quad (2)$$

This gives the indicial lift response to pitching motion as:

$$C_L(s') = C_{L\alpha}(M)\bar{\alpha}\phi_C(s') + \phi_1(s')\bar{\alpha} + \phi_q(s')\bar{q} \quad (3)$$

Where $C_{L\alpha}(M)$ is the lift curve slope for the corresponding Mach number, $\bar{\alpha}$ is the step change in angle of attack defined as the downwash angle ¹ at the

¹Definition?

$\frac{3}{4}c$ position, and \bar{q} is the non-dimensional step change in pitch rate about the $\frac{3}{4}c$ position defined as $\frac{\dot{\theta}c}{U}$. This general form of the indicial lift response can be broken down into the lift due to the impulsive and circulatory components of the response. From (3) the circulatory component of the indicial lift function is given by:

$$\phi_C(s') = 1 - A_1 e^{-b_1 s'} - A_2 e^{-b_2 s'} \quad (4)$$

The impulsive loading contribution to the indicial lift response is represented by the last two terms of equation ² (3). Firstly, the general impulsive component of (3) is given by:

$$\phi_l(s') = \frac{4}{M} e^{\left(\frac{-s'}{T_l'}\right)} \quad (5)$$

Where

$$T_l' = T_l(1 - M^2) \frac{2U}{c} \quad (6)$$

Secondly, the impulsive loading due to the pitch rate about $\frac{3}{4}c$:

$$\phi_q(s') = \frac{-1}{M} e^{\left(\frac{-s'}{T_q}\right)} \quad (7)$$

3 Attached Flow Model

3.1 Numerical Methods

Due to the nature of helicopter rotor aerodynamics, there is a requirement to incorporate both harmonic forcing functions and arbitrary forcing functions into the calculations of rotor load calculations. The harmonic forcing originates from the nature of a rotating blade in a uniform flow field, i.e. the variation of Mach number and hence incidence to avoid unbalanced loading of the rotor disc. The arbitrary forcing comes from the effects of blade vortex interaction which is caused by the vortex shed from the preceding blades

²Definition of T_l, T_q ?

impacting on the following blades. To incorporate these effects, an Indicial Method is used to calculate the harmonic forcing terms for the attached flow regions. A modified Wagner Function [6] is used for this purpose, and the modification incorporates the effects of compressibility. The original Wagner Function was developed to give the unsteady aerodynamic forces on a thin 2-dimensional aerofoil undergoing unsteady motion. The function is only applicable for incompressible flows, and is derived from the impulsive increase in circulation about the aerofoil due to an infinitesimal angle of attack. With the impulsive motion starting from the origin (i.e. when $s = 0$) there is a downwash flow due to the tangential nature of the flow to the aerofoil. This is given by $w = U \sin \alpha \doteq U \alpha$. Assuming that there is a finite velocity at the trailing edge, the circulatory lift is given by:

$$L = 2\pi b \rho U w \phi(s) = 2\pi \frac{c}{2} \rho U U \alpha \phi(s) = (2\pi \alpha) \left(\frac{c}{2} \rho U^2 \right) \phi(s) \quad (8)$$

where

$$\phi(s) = 0 \text{ if } s < 0, \quad s = \frac{Ut}{b} \quad (9)$$

This function can not be used for the calculation of lift in the current form due to the nature of the helicopter operating environments. This is because there are large variations in Mach number from low subsonic at the root to transonic at the tip, and hence effects of compressibility can not be ignored. Also the constant variation in the incidence means that an approximation must be found. The Wagner function is :

$$\phi_c(s) = 1 - A_1 e^{-b_1 s} - A_2 e^{-b_2 s} \quad (10)$$

Where the coefficients are given by [6] such that:

$$\phi_c(s) = 1 - 0.165 e^{-0.0455s} - 0.335 e^{-0.30s} \quad (11)$$

The modification of the Wagner function for compressibility uses the

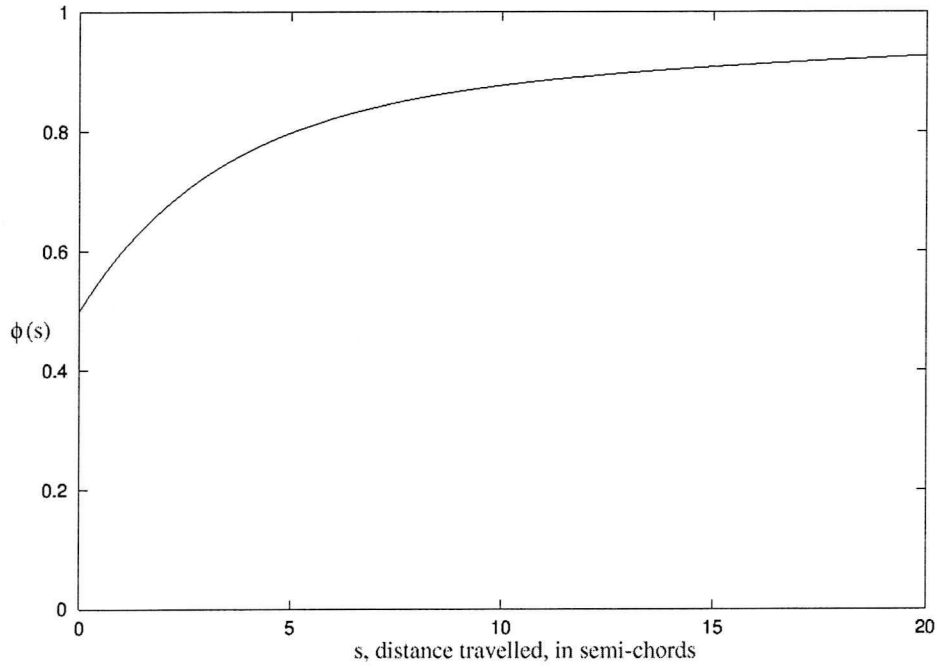


Figure 1: Wagner Function using Coefficients Given by Jones [6]

Prandtl-Glauert [8] transformation approach which results in a modified function:

$$\phi_c(s') = \frac{\phi_c(s)}{\sqrt{1 - M^2}} \quad (12)$$

Using the above modified Wagner function, the lift due to harmonic variations in the incidence ³ of the aerofoil section can be calculated. This is done using equation (8) as follows:

$$C_L = C_{L_\alpha}(M)\Delta\alpha\phi_c(s) \quad (13)$$

since

$$C_L = \left(\frac{L}{\frac{1}{2}\rho c U^2} \right) \quad (14)$$

³For generalised motion, the incidence is taken to be the downwash angle at the $\frac{3}{4}$ chord position

To incorporate the harmonic and arbitrary forcing terms, it is necessary to use an exponential approximation to the Wagner function. This approximation also incorporates the influences of time, and hence covers the hysteresis effects encountered in dynamic systems. The lift is calculated as follows:

$$C_L = C_{L\alpha}(M)\alpha_E(s) \quad (15)$$

Where $\alpha_E(S)$ is given in time as exponential lift decrements:

$$\alpha_E(t) = \alpha_{n=0} + \sum_1^n \left(\Delta\alpha_n - X_n - Y_n \right) \quad (16)$$

Where the exponential lift decrements are given by:

$$X_n = X_{n-1}e^{\frac{-2b_1U\Delta(t)}{c}} + A_1\Delta\alpha_n \quad (17)$$

$$Y_n = Y_{n-1}e^{\frac{-2b_2U\Delta(t)}{c}} + A_2\Delta\alpha_n \quad (18)$$

This approximation also allows for the use of experimental lift curve slope values to be incorporated into the sampling process. For each sampling interval given by:

$$\Delta s' = s(1 - M^2) = \frac{\Delta t(1 - M^2)2U}{c} \quad (19)$$

in real time, it is possible to calculate the lift produced by the aerofoil section. The pitching moment and drag for the attached flow model are calculated by curve fitting experimental data for the relevant incidence. It is also necessary to include the effects of the apparent mass [6] for the system. This produces an additional lift term, and the pitching moment terms. The lift resulting from the apparent mass is given by:

$$L_{AM} = \rho\pi b^2(\ddot{h} - a_h b \ddot{\alpha}) \quad (20)$$

where h is the vertical displacement of the aerofoil section, and α is the rotation of the aerofoil section about an axis a distance a_h away from the

mid-chord position. The pitching moment is also given in this manner:

$$M_{AM} = \frac{-\rho\pi b^4}{8}\ddot{\alpha} \quad (21)$$

Unfortunately, the pitching moment due to the apparent mass is only valid for the incompressible cases, but for simplicity, this term is retained, and modified using the Prandtl-Glauert transformation as before.

This model applies only to attached flow regions of the aerofoil. For helicopter operations near to the flight envelope, there are highly separated regions encountered by the rotors, and hence it is necessary to incorporate the effects of separation using a separate model. Beddoes achieved this using an empirically based Dynamic Stall Model.

4 Dynamic Stall Model

The Calculation method for the rotor loads when the boundary layer over the rotor surface can no longer overcome the adverse pressure gradient due to high incidences, uses an approach based on analysis of large quantities of experimental data. The main dependence of this model is on the static characteristics of the aerofoil sections which in turn depend on the profiles, Mach numbers and Reynolds numbers of the flow conditions. The boundary between the Attached Flow Model and the Dynamic Stall Model is defined by the separation of the boundary layer. This point is demarked by a break in the static aerofoil pitching moment curve which is defined by an incidence α_1 . As separation occurs in a dynamic case, a vortex is shed from the leading edge of the pitching aerofoil, and travels chordwise along the section towards the trailing edge. As this vortex travels, the position of the centre of pressure also travels rearwards. At a second angle of attack α_2 the position of the centre of pressure restabilises, and the lift begins to diverge. From the analysis of experimental data, two time delays demarking firstly the onset of pitching

moment, and secondly the onset of lift divergence have been observed. These time delays are essentially independent of the frequency or amplitude of the harmonic oscillations, aerofoil profile, or flow conditions. Dynamic stall is initiated by separation of the boundary, but for different aerofoil sections, the mechanism of separation is different. Also the effects of supercritical flow influence the separation of the boundary layer.

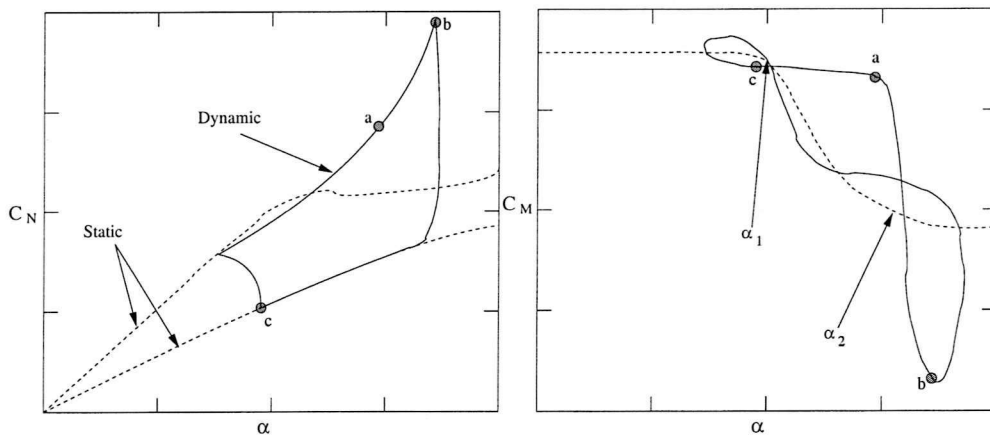


Figure 2: Normal Force and Pitching Moment during Dynamic Stall

4.1 Application of dynamic Stall Model

The approach that the model takes in calculating the lift and pitching moment during dynamic stall of the aerofoil is as follows:

1. As the incidence α increases above α_1 , the Dynamic Stall Model is employed.
 - For a time τ_1 after the static pitching moment break, the lift and pitching moment are calculated as for the attached flow model.
 - After τ_1 , it is assumed that a vortex is shed from the leading edge.

- For a time period τ_2 during which the vortex traverses the chord of the aerofoil, the lift is calculated as for the attached flow model, but the pitching moment diverges, as a result of the movement of the centre of pressure variation caused by the vortex.
- After this second time delay, there is a stabilisation of the centre of pressure, due to the vortex leaving the trailing edge. At this point, there is lift divergence, and a process of reattachment is initiated. This continues until such time as α is less than α_1 when lift and pitching moment are calculated as for the attached flow model.

During the vortex shedding, the centre of pressure is calculated as a function of incidence and time. The representation of the centre of pressure travel is the exponential response to a step change in C_P , and is implemented in the same manner as the Attached Flow Model. The representation of the step input is given by the Laplacian function:

$$f(S) = \frac{1}{(1 + \tau_1 S)(1 + \tau_2 S)} \quad (22)$$

The response to a step input is given by:

$$f(\tau) = \Delta(1 + 3e^{-0.75\tau} - 4e^{-1.3125\tau}) \quad (23)$$

Where the step input Δ is given by:

$$\Delta = C_{P_{new}} - C_{P_{old}} \quad (24)$$

The implementation of this movement of the Centre of Pressure allows the blending between the positions of the Centre of Pressure for attached flow conditions and separated flow conditions between pitching moment divergence, and lift divergence.

5 Region Between Attached and Dynamic Stall Models

There are a number of aspects which define the limits of the dynamic stall region. These include the effects of separation on the lift and pitching moments of the airfoil. Separation can occur in a number of different ways, and most importantly are the effects of leading and trailing edge separation and the effects of shock induced separation.

5.1 Mechanisms of Separation leading to Dynamic Stall

From the studies of Dynamic Stall, two basic mechanisms of separation were identified. Firstly, the stall resulting from the progressive separation of the boundary layer from the trailing edge gives relatively gradual stall characteristics. Secondly, stall resulting from separation of the boundary layer at the leading edge due to separation bubbles failing to re attach has rapid stall characteristics. Leading edge stall characteristics are reproduced efficiently with the Dynamic Stall model, but the trailing edge stall is less well predicted. To overcome this problem:

- The initial angle of attach α_1 is modified to better simulate the effects of dynamic stall resulting from trailing edge separation. This modification is based on observations of dynamic stall during low frequency oscillations.
- A second method of determining the onset of dynamic stall is based on the pressure at the leading edge leading to a pressure criterion which starts the onset of dynamic stall.

This pressure criterion may be used to redefine the initial angle of attach at which the dynamic stall process occurs. It was decided that this criterion

is more appropriate even though it is limited in terms of the range of Mach numbers for which it is applicable. The thinking behind this decision is based on the fact that the process of dynamic stall is most often encountered in the low Mach number range, and hence the criterion applies.

5.2 Trailing Edge Separation

Trailing edge separation is the gradual separation of the boundary layer from the surface of the aerofoil from the trailing edge forwards. This form of separation is gradual in terms of the effect on the lift and pitching moment, and possesses no hysteresis effects [9]. The effect of trailing edge separation causes a loss of circulation which introduces non-linearities into the lift and pitching moments, and also causes a delay to the onset of critical conditions at high incidences. The analytical methods used to incorporate the effects of trailing edge separation into this model are based on the work of Kirchhoff. Kirchhoff developed a relationship between the lift coefficient and the separation point as a function of the chord length.

$$C_L = 2\pi\alpha \left(\frac{1}{2} + \frac{1}{2}f^{\frac{1}{2}} \right)^2 \quad (25)$$

Where f is the location of the separation point non-dimensionalised using the chord length $\left(f = \frac{x}{c} \right)$. This equation applies for a flat plate at incidence, and from this, it is possible to deduce a ratio between the actual lift, and the potential unseparated value.

$$\frac{C_L}{2\pi\alpha} = \frac{1}{4} \left(1 + f^{\frac{1}{2}} \right)^2 \quad (26)$$

From this, it is possible to calculate the separated lift value provided the separation point is known. From experimental data, and assuming that the separation point is defined by the flow reversal point, a relationship between

the separation point and the incidence angle was found. This relationship is simply formed using three defining points, and two exponential curves. The defining points are:

- the fully attached and
- fully separated flow separation points and
- the breakpoint at $f = 0.7$ with the corresponding value of incidence α_1 .

Thus the separation point for an aerofoil at any incidence can be calculated using a curve defined by three parameters:

- α_1 is the incidence defining the breakpoint at $f = 0.7$
- S_1, S_2 are the exponential factors defining the curves from the fully separated and fully attached flow conditions to the breakpoint.

From static test data, it is possible to construct the separation point variation with incidence. The values of $\alpha_1, S_1,$ and S_2 may be curve fitted to these experimental results, and hence the corresponding lift curve calculated for any incidence using (26). It is also possible to calculate the pitching moment variation and drag variation due to the changing separation point. This is achieved by assuming the centre of pressure may be found for any angle of attack from the ratio $\frac{C_M}{C_N}$. The variation is plotted against the corresponding separation point, and a curve of the form:

$$\frac{C_M}{C_N} = k_0 + k_1 f + k_2 f^4 \quad (27)$$

is fitted. This then can be used to find any pitching moment corresponding to an incidence and separation point. The pressure drag is also calculated

in a similar manner, but in this case, there is more emphasis on empirical observations.

$$C_D = C_{D_0} + 0.035C_N \sin \alpha + K_D C_N \sin(\alpha - \alpha_{DD}) \quad (28)$$

Here α_{DD} represents a divergence angle which is obtained from test data for each Mach number. For:

$$\alpha < \alpha_{DD} \quad K_D = 0, \quad \alpha > \alpha_{DD} \quad K_D = 2.7e^{-d_f f} \quad (29)$$

These formulations for forces and moments resulting from the position of the separation point can be extended to cover the effects of trailing edge separation in dynamic flow conditions. From empirical observations of dynamic conditions, it was found that there was a lag between the forward progression of the reversal point, and the static variation with incidence. The behaviour can be represented using a first order lag given by:

$$\frac{f'(p)}{f(p)} = \frac{1}{1 + T_F p} \quad (30)$$

where $f(p)$ is the separation point response to the pressure distribution, and $f'(p)$ incorporates the boundary layer response. From experimental results, the time constant T_F has a value equivalent to 3 semi-chordlengths of travel for $f' < 0.7$. Beyond this point, the reversal speed accelerates, and this is represented by halving the time constant.

The above analysis covers the effects of trailing edge separation on the pressure distribution and moments generated, but this only applies to a certain range of Mach numbers and Reynolds numbers. From test results at moderate Reynolds numbers and for low and high Mach numbers, separation starts at the trailing edge, but may also suddenly start at the leading edge, or at the shock location. This behaviour is represented by methods which are discussed later, and when this occurs, the critical pressure rise method overrides the trailing edge separation method, and the forces and moments are calculated using the critical pressure criterion.

5.3 Critical Pressure Rise

The effects of supercritical flow are incorporated into the model using a pressure criterion based on the shock motion. As the surface flow velocity exceeds the speed of sound, the supersonic region forming on the surface is terminated by a shock wave. As the flow increases in velocity, this region of supersonic flow increases in size, and the terminating shock moves towards the trailing edge. Eventually, the position of the shock will be such that the boundary layer will separate momentarily, and reattach forming a separation bubble. This bubble will increase in size with increasing velocity, and eventually will not be able to reattach, thus resulting in complete separation. Dynamic stall is initiated when this occurs, and this is where the pressure criterion is defined. As separation occurs, the position of the shock moves towards the leading edge under static conditions, and there is a break in the pitching moment, and lift divergence. At this point, the pressure rise across the shock is the criterion at which the dynamic stall process is applied, and the model is used to calculate the resulting lift and pitching moments.

To derive a suitable criterion for the critical pressure rise, it is necessary to know the behaviour of the fluid properties across the shock wave. The governing equations relating to the pressure rise across a shock as presented in [8]:

$$\frac{P_2}{P_1} = \frac{2\gamma}{(\gamma + 1)} M_1^2 \sin^2 \theta - \frac{(\gamma - 1)}{(\gamma + 1)} \quad (31)$$

Which for $\gamma = 1.4$ gives:

$$\frac{P_2}{P_1} = \frac{7M_1^2 \sin^2 \theta - 1}{6} \quad (32)$$

From this we can calculate the pressure rise as a non-dimensional ⁴value as follows:

$$\frac{\Delta P}{P_\infty} = \frac{P_2 - P_1}{P_\infty} = \frac{P_1}{H_0} \left(\frac{P_2}{P_1} - 1 \right) \frac{H_0}{P_\infty} \quad (33)$$

⁴Definition of H_0 ?

$$= \left(\frac{1 + 0.2M_\infty^2}{1 + 0.2M_1^2} \right)^{3.5} \frac{7}{6} (M_1^2 \sin^2 \theta - 1) \quad (34)$$

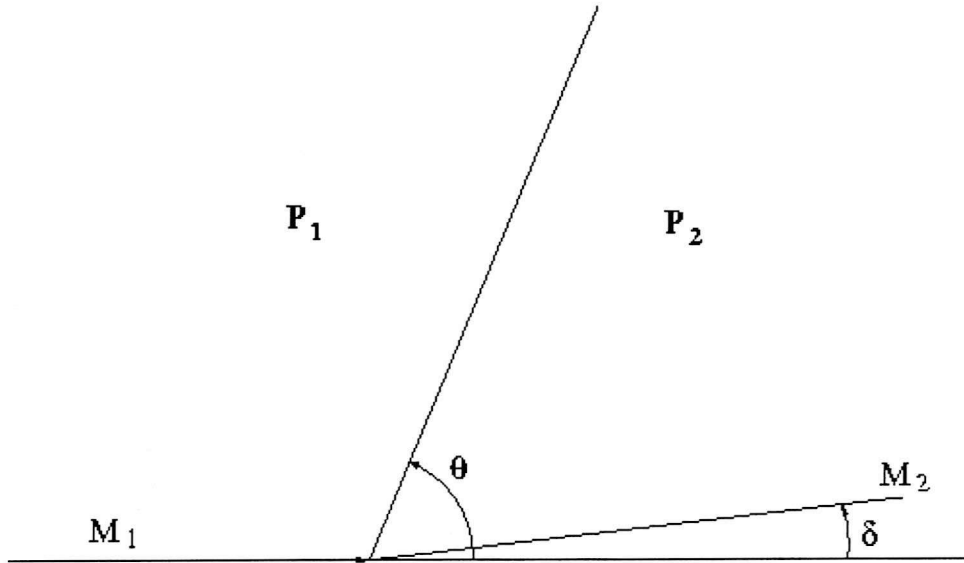


Figure 3: Definition of Shock Parameters

For a supersonic upstream velocity, there is a relationship between the shock angle θ , the velocity deflection angle δ and the upstream Mach number [8]. From this relationship, it is possible to define two flow deflection angles which are of importance to the critical pressure rise. The first deflection angle δ_{max} occurs when the shock becomes oblique, and beyond this point, the flow deflection angle decreases again. The second deflection angle δ^* occurs when the shock become so oblique that the downstream flow velocity is sonic. The differences between these angles are usually small, but when dealing with subsonic freestream cases, sonic flow downstream of a shock is not possible. These angles have been correlated with experimental data, and seem to behave in a similar manner to the pressure rises corresponding to separation bubble formation and shock motion reversal. Thus for a pressure rise of $\frac{\Delta P}{P_\infty} = 0.28$ it is possible to assume that shock reversal and separation

will occur. The correlation between experimental and numerical calculations for this critical pressure rise only apply for freestream Mach numbers above 0.6, but deteriorates below 0.5.

This critical pressure rise criterion can be used for both static and dynamic flow conditions [2]. From experimental results, it was found that there was a phase shift in the lift response followed by a phase shift in the pressure response during dynamic conditions. The final pressure rise at the critical stage before shock reversal was found to be the same for both the static and dynamic cases. Also the onset of pitching moment break occurs at the point when this reversal takes place, hence without further delay.

5.4 Application of the Critical Pressure Rise

It was found there were no significant variations in the critical pressure rise across the shock during shock reversal between the static and dynamic regimes for aerofoil sections. It was also found that the correlation of critical pressure rise across the shock was independent of the profile of the aerofoil. To be able to use the critical pressure rise across the shock as a criterion for finding the pitching moment break defining the dynamic stall region, it is necessary to know the pressure just prior to the shock, and a relationship between the pressure and the normal force C_N . From experimental results, it was found that the phase lag in leading edge pressure with respect to the normal force coefficient is linear, with a time delay equivalent to 1.7 semi-chordlengths of travel. As this relationship is linear, it is possible to relate the pressure as a function of time $P(t)$ and the normal force coefficient as a function of time $C_N(t)$ to the static relation. To avoid calculating the pressures on the surface, it is possible to relate the effects in the changes in pressure to the changes in normal force coefficient. This relationship produces a new normal coefficient C'_N which may be related directly to the variation in pressure and

vice versa. Thus from experimental data, it is possible to find this critical normal coefficient which directly relates to the critical pressure rise across the shock the appropriate Mach number. Using a simple transfer function, the values of C_N and C'_N may be calculated:

$$\frac{C'_N(p)}{C_N(p)} = \frac{1}{1 + T_p p} \quad (35)$$

Where T_p is the time constant equivalent to 1.7 semi chordlengths of travel at a Mach number of 0.3.

This linear relationship is only applicable at low Mach numbers. At higher Mach numbers it becomes non-linear, but the same approach is still appropriate. It was found that the only variation for higher Mach numbers is the value of the time constant. This criterion is useful for both leading edge separation, and shock induced separation.

5.5 Deep Stall and Vortex Shedding

Another phenomenon that occurs during dynamic conditions is stall vortex shedding [2, 5]. As the separation point traverses the chord length, vorticity may be assumed to be shed locally, and convected downstream in the shear layers. When the point is reached that leading edge, or shock induced separation becomes dominant, there is an abrupt change in the location of the separation point, and significant vorticity will be shed in the vicinity of the leading edge. This vorticity will be convected downstream over the upper surface, and in the process cause a large variation in lift. Also, due to the location of the additional lift of the vortex, there will be a large variation in the pitching moment particularly when the vortex leaves the trailing edge.

The vortex lift is calculated as for the lift due to trailing edge separation. Using the Kirchhoff approximation for circulatory lift, the corresponding lift is given by:

$$C_{V_n} = C_{NV_n} (1 - K_{N_n}) \quad (36)$$

Where

$$K_{N_n} = \frac{1}{4} \left(1 + \sqrt{f}\right)^{\frac{1}{2}} \quad (37)$$

The total vortex lift, C_{NV} , is allowed to decay exponentially with time, but may be updated by a new increment in lift:

$$C_{NV_n} = C_{NV_{n-1}} E_v + (C_{V_n} - C_{V_{n-1}}) E_v^{\frac{1}{2}} \quad (38)$$

Where:

$$E_v = e^{\left(\frac{\Delta t}{T_v} \frac{2U}{c}\right)} \quad (39)$$

Thus when the rate of change of lift is low, the vortex lift is being dissipated as fast as it builds up. When the leading edge of pressure rise criterion applies abruptly, there is an rapid build up of vorticity, and this is convected downstream. The rate at which this is convected is determined experimentally. This experimental behaviour has been modeled as:

$$C_{P_V} = \frac{1}{4} \left[1 + \sin \pi \left(\frac{\tau_v}{T_{V_1}} - \frac{1}{2}\right)\right] \quad (40)$$

Where the vortex time $\tau_v = 0$ at the point of vortex shedding from the leading edge, and $\tau_v = T_{V_1}$ when the vortex passes the trailing edge. Thus the change in pitching moment due to vortex lift is given by:

$$C_{MV_n} = C_{P_v} C_{NV_n} \quad (41)$$

The vortex decay constant, T_V , and the centre of pressure travel constant, T_{V_1} are evaluated from experimental data.

5.6 Sweep Effects and Separation Points

The methods outlined so far make use of a strip theory analysis process. This method is suitable for mid-sections of rotors away from either tip effects, but takes no account of the effects of planform changes such as swept rotor tips, or

BERP tip planforms. Using a modified method developed by Kuchemann [7] to analyse wing sweep and tip effects, it is possible to calculate the loading of a rotor blade of arbitrary planform [4]. The original method aimed to modify the lift curve slope using a value derived from the lift achieved at the centre of a doubly infinite swept back wing. From this, a lifting line method was used to find the spanwise lift distribution including the effects of locally induced downwash. For a doubly infinite swept back wing (Λ) the local sectional lift curve slope is given by:

$$C_{L\alpha} = 2\pi\eta \frac{\cos \Lambda}{\sin\left(\frac{\pi\eta}{2}\right)} \quad (42)$$

Where

$$\eta = \left(1 - \frac{\Lambda}{\pi/2}\right) \quad (43)$$

The spanwise variation was achieved by making η a function of the absolute distance y . This also modifies the aerodynamic centre:

$$\eta(y) = \left(1 - \phi(y) \frac{\Lambda}{\pi/2}\right) \quad (44)$$

where

$$\phi(y) = \left(1 + \left(\frac{2\pi y}{c}\right)^2\right)^{\frac{1}{2}} - \frac{2\pi y}{c} \quad (45)$$

The aerodynamic centre as a function of y is given by:

$$\frac{x_{ac}}{c} = \frac{1}{2} \left(1 - \frac{\eta(y)}{2}\right) \quad (46)$$

From these equations, it is possible to calculate the effects of sweep on the lift generated by the rotor sections. To include the effects of the tip, the above equations are used but with the sign of the sweep angle reversed. Thus between these sections, the lift is simply the sum of these two contributions. During the original development of this method, it was found that for low aspect ratio wings, this method was not applicable. To overcome this problem

when considering closely spaced discontinuities in planform it is desirable to minimise the value of $\eta(y)$ as the panel aspect ratio tends to 0. Thus a factor similar to the first order lift curve slope correction is used to eliminate this problem:

$$\eta'(y) = \eta(y) \frac{AR}{1 + AR} \quad (47)$$

With the above equations, it is possible to calculate the effects of arbitrary planforms on the forces and moments generated by the rotor blades.

5.7 Application to Arbitrary Planform Rotor Sections

To apply the above equations to arbitrary planforms, it is necessary to understand that:

- the local sectional lift curve slope is modified using the above sweep laws, and
- the local sectional lift curve slope is further modified due to local kinks in the planform.

Kinks in the planform may be viewed as the centre of a doubly infinite swept back wing of the appropriate sweep angle Λ . Then for the complete rotor, these local kink contributions are simply summed to give the spanwise force distributions. From this it is possible to calculate the effects on the separation point by linking this degree of freedom to the kink factor (η). The square of the kink factor is used to modify the forcing for the separation parameter, and this suppresses the possibility of separation at the centre section. The reverse is true at the tip. The leading edge pressure criterion is also modified in a similar manner.

6 Conclusion

The aerodynamic model developed at WHL to predict unsteady aerodynamic loads on helicopter rotor blades is a quick and efficient design tool. It is capable of predicting the loads under steady and unsteady conditions, and incorporates the effects of dynamic flows. The physical model for predicting dynamic stall is based on empirical observations, and uses static airfoil data to reproduce the effects. Arbitrary forcing is also handled in a step-wise manner allowing for the phenomena of blade vortex interaction to be considered. Further to the original model, a number of improvements were made to allow for more accurate predictions. These include the modeling shock induced separation and leading edge separation using a critical pressure rise criterion. Trailing edge separation, and the effects on the loading of the blade have been included using a modification of the Kirchhoff method. Also the ability to match the loading to the position of the separation point, and predicting when leading edge separation becomes dominant over trailing edge separation during dynamic stall. The effects of vortex shedding on the loading and pitching moments has been included.

The effects of separation in 2-dimensions has been investigated, and extended to 3-dimensions on a finite rotor using a modification of the Kuchemann method. The modifications allow for the prediction of the effects of arbitrary planforms on the loads and moments. The ability to predict any rotor shape extends the capabilities of the code into modern rotor design areas.

While the code is very versatile, and capable of handling a wide range of flow conditions and rotor designs, there are a number of issues that have not been addressed. These include the effects of the true 3-dimensionality on the spanwise load distributions, tip vortex effects on the local loading at the tip, and any later interactions.

References

- [1] Beddoes, T.S. A synthesis of unsteady aerodynamic effects including stall hysteresis. *Vertica*, 1:113–23, 1976.
- [2] Beddoes, T.S. Representation of airfoil behaviour. *Vertica*, 7(2):183–97, 1983.
- [3] Beddoes, T.S. Practical computation of unsteady lift. *Vertica*, 8(1):55–71, 1984.
- [4] Beddoes, T.S. A 3-D separation model for arbitrary planforms. In *47th. Annual Forum of the American Helicopter Society*, 1991.
- [5] Beddoes, T.S., Leishman, J.G. A generalised model for airfoil unsteady aerodynamic behaviour and dynamic stall using the indicial method. In *42nd. Annual Forum of the American Helicopter Society*, 1986.
- [6] Fung, Y.C. '*An Introduction to the Theory of Aeroelasticity*'. Dover Publications, Inc. New York, 2nd edition, 1993.
- [7] Küchemann, D. *The Aerodynamic Design of Aircraft*. Pergamon Press Ltd., UK, 1st edition, 1978.
- [8] Kuethe, A.M., Chow, C-Y. '*Foundations of Aerodynamics*'. John Wiley and Sons, Inc. New York, 5th edition, 1998.
- [9] Prouty, Raymond W. '*Helicopter Performance, Stability, and Control*'. PWS Publishers, Boston, USA, 1st edition, 1986.

